Semi-Automatic Aortic Aneurysm Analysis

Osman Bodur[1], Leo Grady[1], Arthur Stillman[2], Randolph Setser[3], Gareth Funka-Lea[1], Thomas O'Donnell[1]

[1] Siemens Corporate Research, Princeton, NJ 08540
[2] Emory University Hospital, Atlanta, GA 30322
[3] Cleveland Clinic Foundation, Cleveland, OH 44195

Aortic aneurysms are the 13th leading cause of death in the United States. In standard clinical practice, assessing the progression of disease in the aorta, as well as the risk of aneurysm rupture, is based on measurements of aortic diameter. We propose a method for automatically segmenting the aortic vessel border allowing the calculation of aortic diameters on CTA acquisitions which is accurate and fast, allowing clinicians more time for their evaluations. While segmentation of aortic lumen is straightforward in CTA, segmentation of the outer vessel wall (epithelial layer) in a diseased aorta is difficult; furthermore, no clinical tool currently exists to perform this task. The difficulties are due to the similarities in intensity of surrounding tissue (and thrombus due to lack of contrast agent uptake), as well as the complications from bright calcium deposits.

Our overall method makes use of a centerline for the purpose of resampling the image volume into slices orthogonal to the vessel path. This centerline is computed semi-automatically via a distance transform. The difficult task of automatically segmenting the aortic border on the orthogonal slices is performed via a novel variation of the isoperimetric algorithm which incorporates circular constraints (priors). Our method is embodied in a prototype which allows the loading and registration of two datasets simultaneously, facilitating longitudinal comparisons. Both the centerline and border segmentation algorithms were evaluated on four patients, each with two volumes acquired 6 months to 1.5 years apart, for a total of eight datasets. Results showed good agreement with clinicians' findings.

1 Introduction

The aorta is the largest artery in the body and is the primary conduit of oxygenated blood. An Aortic Aneurysm (AA) is a permanent and irreversible localized dilation of this vessel and, if left untreated, will gradually expand until rupture, resulting in death in 90% of cases [1]. AAs are the 13th leading cause of death in the United States. [2].

Treatment for this disorder, such as open surgical repair, runs significant risk including infection, pseudoaneurysm formation, and secondary impotence [3]. although endovascular stent repair is gaining popularity, the long term outcome of this procedure is not yet known [4] and not all AAs are candidates for stents [2]. Therefore, for AAs *not* thought to be an imminent rupture risk, surveillance is

considered preferable to immediate aggressive treatment. This is particularly true in the largest population affected by this disorder, men over 65 years of age [2], since morbidity from other causes may occur prior to rupture.

How to determine the rupture risk of an AA, though, is still an open question. Proposed indicators are manifold: wall stress, wall stiffness, intraluminal thrombus thickness, and wall tension have all been suggested [1]. Standard procedure, however, calls for intervention (open repair or stent) when the maximal diameter is greater than 5.5cm [2]. (The change over time of the maximal diameter has also been put forth as a prognostic measure [3]).

The goal of our work was the development of a tool for fast, accurate assessment of aortic diameters as well as providing a basis for the exploration of alternative or complementary indicators of rupture risk.

Currently there are two common approaches to aortic diameter measurement. The first involves making linear measurements on a Maximum Intensity Projection (MIP) of the image volume. However, the selection of MIP projection angle may introduce a high degree of subjectivity in this measurement. The second employs a double oblique multi-planar reformat (MPR) to obtain a reconstructed image orthogonal to the vessel path on which measurements are made. The drawback of this approach is that it is time consuming and as a result the aorta may be sparsely sampled due to practical limits on the duration of analysis. In addition, when performed manually, the orthogonal plane may not be correct, introducing error. Reproducing the same orthogonal cross-section position in a longitudinal study may also prove difficult. Finally, the manual measurement made may not be correct as it relies on the user subjectively determining which points are connected to form the maximal diameter.

Our approach is to semi-automatically determine the centerline of the aorta (lumen) and reconstruct a series of images orthogonal to this centerline. We then automatically segment these vessel cross-sections with a modified isoperimetric segmentation algorithm. Due to the difficulties introduced by thrombi, calcifications, and the similarity in gray scale between the vessel wall and surrounding structures, we provide for the editing of the segmentations. From the edited segmentations we then construct a 3D model of the aorta. Finally, we allow for the registration of two image volumes facilitating follow-up studies.

There are several advantages to our approach. First, it is possible to get a complete coverage of the aorta. It is not unusual for a physician user to be constrained to only a few minutes to examine a study. Using our system, within seconds the clinician has access to a series of optimal, reproducible, orthogonal cross-sections of the entire vessel which may be visually inspected for any irregularities. Further, the user can segment these cross-sections and have the guaranteed maximal diameter automatically computed. After the 3D model is constructed, stent planning is possible and we set the stage to compute rupture risk indicators such as wall stress (in conjunction with blood pressure readings). Finally, via registration, side by side comparison of the same aorta at different time points becomes straightforward. Since the monitoring of both AAs at risk, as well as repaired aortas is commonplace [5] this feature becomes quite valuable.

2 Related Work

Loncaric et. al.,[6] use 3D level sets to segment the lumen as well as vessel border. For the vessel border they employ a stopping criterion based on the assumption that the aortic surface is smooth and round. We also employ a circularity constraint. Ours, however, solves for an exact global energy function and is not susceptible to local minima. Subramanyan et. al.,[7] also use 3D level sets but do not provide details on how they detect the vessel border. Both Loncaric and Subramanyan create centerlines to compute orthogonal MPRs.

De Bruijne et. al.,[8] apply a novel active shape model formulation in which landmarks may be defined by correlating with adjacent slices rather than training data. The model is initialized manually and their two-slice model climbs one slice at a time along the aorta. They focus on abdominal aorta where the central axis of the vessel is approximately perpendicular to the image stack and therefore do not require a centerline calculation. Their approach, however, requires a training set and runs the risk of degenerating modes of variation since the aortic cross-sections are frequently circular.

Both Fillinger [5,9,10] and Vorp [1,11] construct 3D finite element models (FEM) of the aorta. Fillinger [10] requires 2-4 hours for model construction, although they do include branch vessels and perform a mesh-refinement. However, segmentation details are not included. In Vorp [11], it is assumed that the segmentations of the outer wall are manual.

Hernandez et. al., [12] segment aneurysms in the brain using a Geodesic Active Region Model combined with non-parametric region-based information. In this domain, however, the challenges come in the morphology of the vessel; the brain vasculature being more detailed and complex as compared to the aorta. The authors do not address the issue of thrombi.

Olabarriaga et. al., [16, 17] employ a 3D deformable model to segment the epithelial layer of thrombotic aortic aneurysms. An active shape model approach is used to learn the profiles perpendicular to the vessel wall. K nearest neighbors classifies a point as inside, outside, or on the border. This classification is transformed into an external force attracting the model to the epithelial layer.

3 Methods

3.1 Centerline Finding

The initialization to our centerline computation is given interactively by two user-defined points, one at the base of the aorta, and the other near the iliac bifurcation. From these two points, a histogram of the lumen intensities is calculated using a standard Gaussian kernel estimator on the distribution of intensities in a small neighborhood of the input points. Following the lumen intensity estimation, the

voxels in the volume are thresholded against the likelihood that each voxel intensity belongs to the aortic lumen. A distance transform is computed on the thresholded volume and a distance tree is computed [13]. Within any tree, there is a unique path between any two points. The path between the two input points in the distance tree is output as the aortic lumen centerline, which is subsequently smoothed.

The image volume is resampled into a series of MPRs normal to the centerline. The intersection of the centerline with these images forms a point in the center of the lumen. This serves as input to the segmentation of the aortic border.

3.2 Aortic Cross-section Segmentation

To determine the maximal aortic diameter we must segment the entire vessel border. Segmentation of this border, in the presence of thrombus, is an extremely difficult problem due to the bimodal distribution of intensities within the aorta (including sharp internal boundaries) and the presence of nearby confounding structures such as the diaphragm, veins and branch vessels.

The design of our segmentation approach takes into consideration the following factors:

1. Lumen and thrombus intensities may be estimated.
2. An algorithm capable of cutting weakly-connected confounding structures must be employed.
3. The aortic cross-sections may be assumed to be generally circular.
4. A point in the lumen from the centerline intersection is available.

For the present task, the isoperimetric segmentation algorithm of [14] appeared as a good candidate, since it takes input as a single point and was shown to correctly cut weakly-connected confounding structures. However, this algorithm does not encourage circularity of the segmentation (on a weighted graph) and therefore requires modification.

To begin, a K-means algorithm is employed to cluster distinct intensity groups within the image. We use K=5, and select the means corresponding to the lumen intensity (known from the location of the centerline point) and the thrombus, by looking for a mean that is nearby to the centerline (but not belonging to the lumen mean). We reject the mean as not representing a thrombus if the number of voxels belonging to the mean is too small or if the means falls outside a learned range of plausible thrombus intensities.

Modified Isoperimetric Algorithm

The isoperimetric segmentation algorithm of [14] attempts to minimize the ratio

$$h(x) = \frac{x^T L x}{x^T d}$$

for an indicator function, x, on the set of nodes (pixels) with a weighted Laplacian, L, where d is the sum of incident edge weights on a node (see [14] for details of these definitions). For an estimated distribution for lumen, D_L and thrombus D_T, the weights (affinities) between neighboring pixels, i and j, are given by

$$w_{ij} = e^{-(D_L(i)+D_T(i)-D_L(j)-D_T(j))^2}$$

In [15], it was shown that the solution given by the minimization of *h(x,)* above, with uniform incident weights leads to a circle – the classical solution of the isoperimetric problem from which the algorithm was motivated. Therefore, one may combine the above term from the isoperimetric algorithm and add to it a circularity term to produce the joint minimization[1]

$$g(x) = \frac{x^T L x}{x^T d} + \gamma \frac{x^T U x}{x^T u},$$

where U indicates a Laplacian matrix with uniform weights and u represents the vector of uniform value incident edges. The joint minimization of *g(x)* ultimately leads to the solution of the standard isoperimetric algorithm, with the weights modified by adding a constant γ to each weight. The parameter γ controls the level of circularity enforced on the solution, with γ=0 representing no preference for circles and γ=∞ forcing the solution to be a circle, regardless of the image content. For our purposes, we found that a good balance could be achieved by setting γ=0.03.

Figure 1 shows the segmentation process. The left image shows the input image, the center image shows the (combined) probability map that the pixels belong to the aorta (upon which the weights are based, i.e., this is the image passed to the modified isoperimetric algorithm) and the rightmost image displays the segmentation, where the blue/gray spot indicates the input location of the centerline and the orange/light gray ring indicates the location of the resulting segmentation border. Note that the rightmost image has been whitened to enhance contrast with the segmentation.

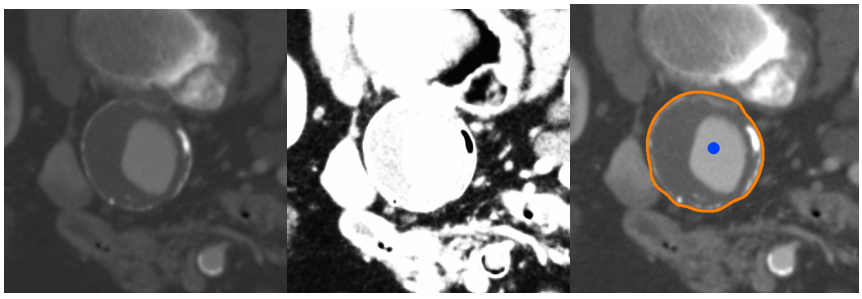

[1] 4/20/07 LJG – The equation is given here as published. However, this equation was not correctly written. Instead, it should read: $g(x) = \frac{x^T (L + \gamma U) x}{x^T (d + \gamma u)}$

Fig. 1 Left: A cross-sectional image of an aorta exhibiting thrombosis. Middle: Map showing probability that a pixel belongs to the aorta. Right: Segmentation of the image with initial centerpoint included.

4. Results

For in vitro validation of the centerline algorithm, a static, fluid-filled aorta phantom was built using an approximately 4 foot long segment of Tygon vinyl tubing (1 inch inner diameter, 1.25 inch outer diameter) bent at a 180 degree angle at its mid-section to simulate the human aorta. The phantom was filled with a solution of water and gadolinium contrast (Magnevist, Berlex) (approximately 1 ml contrast per 15 ml water) and placed on the bed of the CT scanner (Sensation 64, Siemens). A contrast-enhanced, non-gated spiral examination was used to reconstruct non-overlapping, 3 mm thick slices. The phantom cross-section was measured in four places: base (orthogonal to image stack – 0 degrees), 45 degrees (towards peak bend), 90 degrees (peak), and 135 degrees (away from peak bend), and compared to measurements made using our prototype. On average, the RMS difference between these values was 1.5mm.

We validated both our centerline and segmentation algorithms on four patients with two image volumes each (Time1 and Time2) acquired six months to 1.5 years apart. Patients were imaged at least twice between February 2002 through December 2005 using 4-slice (Volume Zoom, Siemens Medical Solutions), 16-slice (Sensation 16, Siemens) and/or a 64-slice (Sensation 64, Siemens) CT system. The same imaging parameters described above were used.

An expert radiologist reformatted the Time1 datasets manually (via double oblique reformat) to obtain cross-sections, and measured aortic diameters manually (Manual Cross-section/Manual Diameter, abrev: Man X/Man Diam) using virtual calipers at 9 points along the aorta. We then loaded both Time1 and Time2 datasets into our prototype, registered them, and created a centerline. The expert scrolled through the automatically generated cross-sections to approximately the same points as measured previously and manually determined diameters (Auto Cross-section/Manual Diameter, abrev: Auto X/Man Diam) as well as generating automatic diameters (Auto Cross-section/Auto Diameter, abrev: Auto X/Auto Diam) on both time points. We show an example dataset for one patient in Table 1. The 3D model constructed from this patient is shown in Figure 2.

	Time 1:Man X/Man Diam	Time 1: Auto X/Man Diam	Time 1: Auto X/Auto Diam	Time2: Auto X/Man Diam	Time2: Auto X/Auto Diam
aortic root	3.3 cm	3 cm	3.7 cm	2.8 cm	3.2 cm
mid-ascending	3.5 cm	3.3 cm	3.2 cm	3.2 cm	3.5 cm
proximal aorta	2.9 cm	3.1 cm	3.4 cm	3 cm	3.4 cm
ithmus	2.7 cm	2.8 cm	3 cm	2.9 cm	3.5 cm
mid-descending	5.5 cm	5.7 cm	5.1 cm	5.8 cm	5.5 cm
lower thoracic	6 cm	5.8 cm	6.7 cm	5.9 cm	6.5 cm
ciliac origin	3.3 cm	3 cm	3.9 cm	3.2 cm	3.9 cm
renal segment	3.3 cm	3.1 cm	3.1 cm	3 cm	3.4 cm
infrarenal	2.9 cm	2.9 cm	3.1 cm	2.8 cm	3.6 cm

Table 1. Sample results for evaluation of prototype. Column1: Manual Cross-section/Manual Diameter Measurement on Time 1 image volume. Column2: Automatic Cross-section/Manual Diameter Measurement on Time 1 image volume. Other columns similarly headed.

The average difference between Man X/Man Diam and Auto X/Man Diam for Time 1 over all patients was .197 ± .152cm. The signed difference was .136 ± .209cm with the Man X/Man Diam on average larger. This indicates that our automatic centerline method was on average better at finding the orthogonal image plane to the vessel (measurement of the vessel diameter is never smaller than in the true orthogonal cross-section). The difference over all image volumes for Auto X/Man Diam and Auto X/Auto Diam was .342 ± .245. Each image required .52 edits on average.

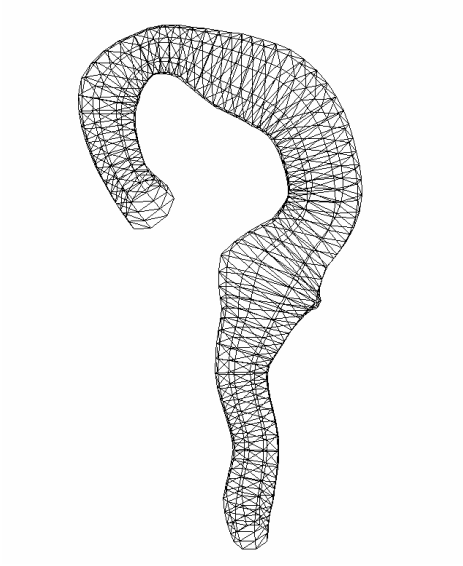

Fig. 2. The reconstructed aorta from Table1.

5 Conclusions

We have motivated the need for tools to assess the size and rupture risk of aortic aneurysms. Also, we have demonstrated a method by which aortic diameters, currently the standard means by which this is judged, may be accurately evaluated.

It should be pointed out that our approach also yields a significant time savings over standard analysis techniques. On average, it took our expert radiologist approximately 15 minutes to perform the manual double oblique sampling of a single dataset. With our prototype, he was able to visually analyze and make measurements on *two* image acquisitions from the same patient in 10 minutes – and, with complete coverage of the aorta.

The points chosen for comparison by our expert radiologist were often located near bifurcations off the aorta. These bifurcation points make it easier to consistently compare the same location when performing a manual analysis but make the automatic segmentation more tricky since the segmentation can bleed into the adjoining vessel.

In the future, we hope to apply our prototype to the search for rupture risk indicators. With the creation of our 3D models, it becomes possible to evaluate the efficacy of wall stress, wall stiffness, etc., as well as volumetric features. In addition, we have the option to explore dynamic characteristics of the aorta given our registration component.

Acknowledgements

The authors would like to thank Stacie Kuzmiak, R.T. for acquiring the phantom data.

References

[1] Vorp, David et. al., "Biomechanical Determinants of Abdominal Aortic Aneurysm Rupture", Arteriosclerosis, Thrombosis, and Vascular Biology, Journal of the AHA 2005;25;1558-1566.

[2] Sakalihasan N, et. al., "Abdominal Aortic Aneurysm" Lancet 2005; 365: 1577-89

[3] Limet R, Sakalihassan N, Albert A, "Determination of the expansion rate and incidence of rupture of abdominal aortic aneurysms," J Vascular Surgery 14(4) Oct 1991, pp 540-548.

[4] Therasse E, Soulez G, Giroux M-F, Perreault P, et. al. "Stent-Graft Placement for the Treatment of Thoracic Aortic Diseases", Radiographics 2005 25: pp 157-173.

[5] Fillinger, M, "New Imaging Techniques in Endovascular Surgery," Surgical Clinics of North America 79(3), pp 451-75, June 1999.

[6] Loncaric S, Subasic M, Sorantin E , "3-D Deformable Model for Abdominal Aortic Aneurysm Segmentation from CT Images," First Int'l Workshop on Image and Signal Processing and Analysis, pp 139-144, June 2000, Pula Croatia.

[7] Subramanyan K, et. al., "Automatic Aortic Vessel Tree Extraction and Thrombus Detection in Multi-Slice CT", Medical Imaging 2003: Image Processing, Proc SPIE Vol. 5032.

[8] de Bruijne et. al., "Interactive Segmentation of Abdominal Aortic Aneurysms in CTA Images", Medical Image Analysis 8(2) pp 127-158.

[9] Fillinger M, Raghavan M L, et. al., "In vivo analysis of mechanical wall stress and abdominal rupture risk", J Vascular Surgery, pp. 589-597. Sept 2002.

[10] Fillinger M, Marra S, Rghava M L, Kennedy F, "Prediction of rupture risk in abdominal aortic aneurysm during observation: Wall stress versus diameter," J Vascular Surgery, 37(4), pp 724-732, April 2003.

[11] Sacks M, Vorp D, Raghavan M L, Federle M, Webster M, "*In Vivo* Three-Dimensional Surface Geometry of Abdominal Aortic Aneurysms," Annal Biomed Eng 27, pp 469-479, 1999.

[12] Hernandez M, Frangi A, Sapiro G, "Three-Dimensional Segmentation of Brain Aneurysms in CTA Using Non-parametric Region-based Information and Implicit Deformable Models: Method and Evaluation," MICCAI 2003 pp 594-602, 2003.

[13] Grady L., "Fast, Quality, Segmentation of Large Volumes ---Isoperimetric Distance Trees", ECCV 2006, pp 449-462.

[14] Leo Grady and Eric L. Schwartz, "Isoperimetric Graph Partitioning for Image Segmentation", IEEE Trans. on Pattern Analysis and Machine Intelligence, vol. 28, no. 3, pp. 469-475, March 2006.

[15] Leo Grady and Eric L. Schwartz, "Isoperimetric Partitioning: A new algorithm for graph partitioning", SIAM Journal on Scientific Computing, vol. 27, no. 6, pp. 1844-1866, June 2006.

[16] Olabarriaga S., Rouet J.-M., Fradkin M,. "Segmentation of Thrombus in Abdominal Aortic Aneurysms from CTA with Non-Parametric Statistical Grey Level Appearance Modelling, " *IEEE Transactions on Medical Imaging*, 2005, v. 24, n. 4, p. 477-485.

[17] S.D. Olabarriaga, M. Breeuwer, W.J. Niessen, "Multi-scale Statistical Grey Value Modelling for Thrombus Segmentation from CTA", in: *Medical Image Computing and Computer-Assisted Intervention*, Springer, 2004, vol. 3216, Lecture Notes in Computer Science, p. 467-474.